Power Analysis and Maximum Output-Power Scheme for Inductively Coupled Resonant Power Receivers

Nan Xing, *Graduate Student Member, IEEE,* and Gabriel A. Rincón-Mora, *Fellow, IEEE*
Georgia Institute of Technology, Atlanta, Georgia 30332 U.S.A.
nxing3@gatech.edu and Rincon-Mora@gatech.edu

***Abstract*— Although microsensors nowadays can save money, energy, and lives, highly functional devices can exhaust a tiny battery very quickly. Harvesting ambient energy can help replenish the battery, but only when an ambient source is available. Unfortunately, many embedded microsensors are small, stationary, and enclosed, so thermal gradients, motion, and light are absent. Wireless power in these cases is often the only option left. But since the receiving coil is small and centimeters away from the transmitter, drawn power is low. Switched resonant bridges are popular in this respect because they output more power with fewer components than their non-switched and non-resonant counterparts. But still, power can be so low that losses can be overwhelming. This paper introduces a power analysis and proposes a skipping collection scheme that boosts output power. Analysis and simulations show how switched resonant bridges consume conduction and switching power and how dispersing collection times can boost output power.**

***Index Terms*—Maximum wireless power, inductively coupled receiver, damping energy, embedded microsensor, battery charger.**

I. Inductively Coupled Microsystems

Microsensors can sense, process, and transmit information that can save money, energy, and lives. Onboard sensors, interface electronics, data converters, microprocessors, and power amplifiers, however, require power levels that tiny batteries cannot sustain for long. Harvesting ambient energy can help, but only when available, and only to the extent small transducers can. Unfortunately, microsystems embedded in the body, walls, and equipment hardly move or receive light. And the temperature across these millimeter devices is so low that thermoelectric generators output less than 15 nW/mm^3 [1].

The only option left for many of these tiny devices is wireless inductively coupled power [2]–[7]. Except, power transmitters are not always nearby. So to survive long drought periods between sporadic recharge events, receivers should draw as much power from as far a source as possible. Although resonant and switched bridges can draw as much power, only switched resonant bridges exclude a separate charger stage that occupies space and dissipates power [8].

So the underlying purpose of the switched resonant bridge in Fig. 1 is to replenish the battery v_{BAT} [8] with the most power, the least space, and the farthest source possible. For this, the transmitting source v_T and the tuned L_T–C_T filter produce an alternating current in the transmitting coil L_T. This establishes a changing magnetic field that reaches the receiving coil L_R. The captured field then induces an EMF voltage $v_{EMF.R}$ in L_R from which the bridge draws power to replenish v_{BAT}. The bridge can viably power the system directly. But without v_{BAT}, the system cannot function between recharge cycles. With v_{BAT}, on the other hand, v_{BAT} stores excess energy that the regulating power supply can tap to feed system components when transmitting sources are absent.

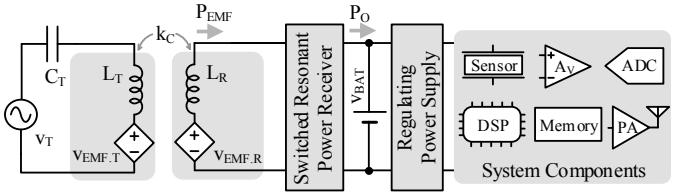

Fig. 1. Inductively powered microsystem.

These systems are usually very small and centimeters away from any source. L_R therefore captures a small fraction of the magnetic flux that L_T produces. With such a low coupling factor k_C, L_R draws little EMF power P_{EMF}. So little, in fact, that power losses in the receiver can overwhelm P_{EMF} to such a degree that output power P_O can altogether fade to zero.

This paper proposes a skipping collection scheme in Section II that saves more than it sacrifices when EMF power is low. Sections III and IV then introduce a new power analysis that can quantify these savings. And Sections V and VI show and discuss how output power is higher as a result.

II. Proposed Skipping Collection Scheme

A. Switched Resonant Bridge

A resonant bridge incorporates a capacitor C_R that together with the receiver coil L_R resonate at the operating frequency f_O of the transmitter. Induced EMF voltage $v_{EMF.R}$ and L_R's current i_L are therefore in phase: both positive or both negative. As a result, $v_{EMF.R}$ continually sources power, so the energy that C_R and L_R exchange grows over time. Switch S_R in Fig. 2 closes for this purpose, to resonate the L_R–C_R tank [9].

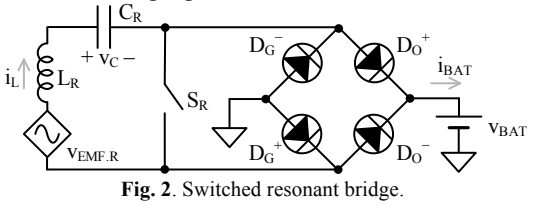

Fig. 2. Switched resonant bridge.

The purpose of the bridge is to *bleed* excess energy from the tank into the battery v_{BAT}. So whenever S_R opens, diodes D_G^+–D_O^+ or D_G^-–D_O^- steer i_L momentarily into v_{BAT}. In steady state, L_R and C_R replenish each other and the bridge draws the EMF power P_{EMF} that $v_{EMF.R}$ supplies.

Luckily, incorporating S_R's functionality into the ground diodes D_G^+ and D_G^- like Fig. 3 shows [10]–[11] is

straightforward because D_G^+, D_G^-, D_O^+, and D_O^- are in practice MOS transistors that switch like diodes [12]–[13]. So with fewer switches, M_G^+ and M_G^- incorporate S_R and M_O^+ and M_O^- operate like diodes. Here, M_G^+ *and* M_G^- close to resonate the tank and M_G^+ *or* M_G^- open to bleed i_L into v_{BAT}.

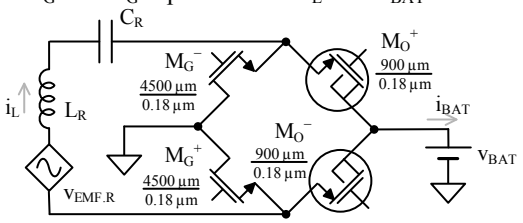

Fig. 3. Four-switch variation of the switched resonant bridge.

B. Continual Collection Scheme

Switched resonant bridges normally collect energy every half cycle [9]–[11]. Although collection can happen at any point, drawing EMF power P_{EMF} when the receiving coil's current i_L is at its highest point collects the most energy across the shortest time. A short collection time t_C is important because the disruption in the cycle tends to detune the filter, which reduces drawn power. But t_C can be so short when i_L is at its peak $i_{L(PK)}$ that the distortion can be minimal.

In the simulation of Fig. 4, for example, L_R's 4.7 µH and C_R's 117 pF oscillate and exchange energy at 6.78 MHz. So when C_R's energy maxes, its voltage v_C peaks to 2.8 V and L_R's current i_L, which reflects L_R's energy, is zero. Similarly, L_R's energy and current peak at 14.2 mA when v_C crosses 0 V. Steering 14.2 mA into a 1.8-V battery v_{BAT} every half cycle $0.5T_O$ for 1.4 ns of the 147-ns period T_O outputs 176 µW:

$$P_O = P_{EMF} - P_{LOSS} = i_{BAT} v_{BAT} \left(\frac{t_C}{0.5T_O} \right). \quad (1)$$

So to fully replenish the tank every half cycle, P_{EMF} supplies 176 µW *plus* all the power that the system loses as P_{LOSS}.

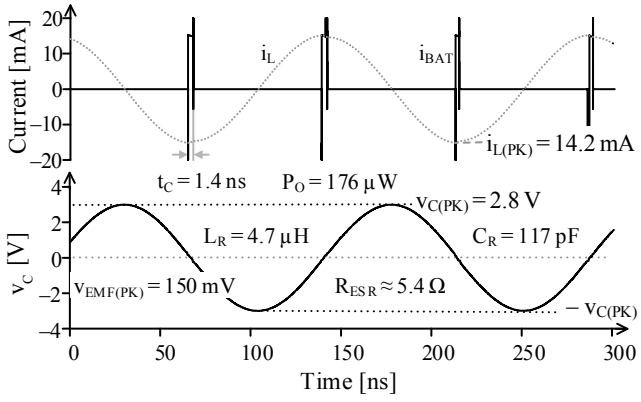

Fig. 4. Simulated waveforms when collecting energy every half cycle.

When the receiving coil L_R is small and distant, L_R captures a small fraction of the magnetic field that the transmitter coil L_T generates. P_{EMF} can be so low that P_{LOSS} can overwhelm P_{EMF}. In other words, drawing power can drain the tank more than P_{EMF} can replenish. So oscillations fade until P_{EMF} can sustain P_{LOSS}.

Luckily, conduction power P_R scales down with P_{EMF}. But since collection frequency f_C does not, switching losses P_{SW} do not. So to output P_O, P_{EMF} must overcome P_{SW} at f_C, which here is twice the power-band frequency f_O or 13.56 MHz.

C. Proposed Skipping Collection Scheme

One way to reduce this power threshold is to reduce the collection frequency f_C. For this, the power receiver can skip N_S half cycles before every collection. In Fig. 5, for example, the receiver skips 3 half cycles. Since the tank accumulates the EMF energy that $v_{EMF.R}$ supplies, output power P_O is not lower than when collecting every half cycle. Switching losses P_{SW}, however, are 4× lower, so P_{EMF} must overcome considerably less P_{SW} to output 2.7× more power: 478 µW.

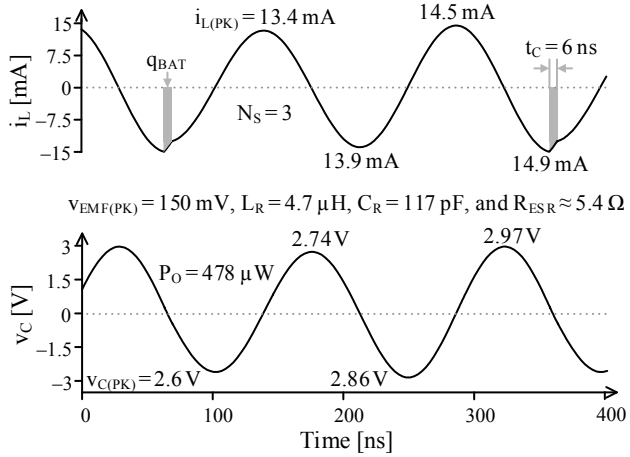

Fig. 5. Simulated waveforms when skipping three half cycles.

Since $v_{EMF.R}$ always supplies power, tank energy climbs across uncollected half cycles. As a result, C_R's and L_R's peak voltages and currents $v_{C(PK)}$ and $i_{L(PK)}$ climb across uncollected half cycles until a collection event resets them to their initial levels. This is why $v_{C(PK)}$ and $i_{L(PK)}$ in Fig. 5 grow from 2.6 to 2.97 V and 13.4 to 14.9 mA between collection events.

III. Power Analysis

A. Power Drawn

When tuned, induced EMF voltage $v_{EMF.R}$ and the receiving coil L_R's current i_L are in phase. $v_{EMF.R}$ therefore sources EMF power P_{EMF} continually across every half cycle. i_L's peak $i_{L(PK)}$ roughly corresponds to C_R's peak $v_{C(PK)}$ because L_R and C_R exchange their $0.5C_R v_{C(PK)}^2$ and $0.5L_R i_{L(PK)}^2$ energies. So $v_{EMF.R}$'s and $i_{L(RMS)}$'s sinusoids generate P_{EMF}':

$$P_{EMF}' = i_{L(RMS)} v_{EMF.R(RMS)} \approx \left(\frac{v_{C(PK)}}{\sqrt{2}} \sqrt{\frac{C_R}{L_R}} \right) \left(\frac{v_{EMF(PK)}}{\sqrt{2}} \right). \quad (2)$$

In Fig. 4, for example, P_{EMF}' is 1.12 mW with 4.7 µH and 117 pF when $v_{EMF.R}$ peaks to 150 mV at 6.78 MHz. When skipping half cycles, however, $v_{C(PK)}$ rises after every uncollected half cycle. So on average, $v_{EMF.R}$ supplies the averaged sum P_{EMF}:

$$P_{EMF} = \left(\frac{1}{N_S + 1} \right) \sum_{k=1}^{N_S+1} P_{EMF(k)}'. \quad (3)$$

B. Power Losses

Unfortunately, a number of loss mechanisms deduct power. For one, as already mentioned, the power receiver consumes conduction and switching power P_R and P_{SW}. But what is

perhaps less obvious is the power sacrificed when skipping half cycles, which constitutes another loss.

Conduction Loss: Parasitic resistances in the receiver coil L_R, resonant capacitor C_R, and switches M_G^+, M_G^-, M_O^+, and M_O^- burn ohmic power when they conduct i_L. When combined and averaged across a half cycle, they present an equivalent series resistance R_{ESR} (of 5.4 Ω in Fig. 3) that burns P_R':

$$P_R' = i_{L(RMS)}^2 R_{ESR} = \left(\frac{v_{C(PK)}}{\sqrt{2}}\sqrt{\frac{C_R}{L_R}}\right)^2 R_{ESR}. \quad (4)$$

But since $v_{C(PK)}$ rises after every uncollected half cycle, R_{ESR} burns the averaged sum P_R:

$$P_R = \left(\frac{1}{N_S+1}\right)\sum_{k=1}^{N_S+1} P_{R(k)}'. \quad (5)$$

Switching Loss: Gate–source and gate–drain capacitances in M_G^+, M_G^-, M_O^+, and M_O^- require energy to charge. When combined, the system supplies energy $q_C\Delta v_C$ or $C_{PAR}\Delta v_C^2$ to charge C_{PAR}'s 4.7 pF across Δv_C's 1.8 V. Since the receiver skips N_S half cycles, C_{PAR} draws an $N_S + 1$ fraction as P_{SW}:

$$P_{SW} = C_{PAR}\Delta v_C^2\left(\frac{f_C}{N_S+1}\right) = C_{PAR}\Delta v_C^2\left(\frac{2f_O}{N_S+1}\right). \quad (6)$$

In steering this power, transistors in the drivers burn P_{SW} like the switches in Fig. 3 burn P_R: in the form of heat.

Sacrificial Loss: Although P_{EMF} and P_R both scale with $i_{L(RMS)}$, P_{EMF} climbs with $i_{L(RMS)}$ and P_R with $i_{L(RMS)}^2$. So added quadratic losses ΔP_R start outpacing linear gains ΔP_{EMF} after the peak voltage $v_{C(PK)}$ that corresponds to $i_{L(PK)}$ surpasses [7]

$$v_{MPP0} = v_{C(PK)}\big|_{MPP} = \frac{v_{EMF(PK)}}{2R_{ESR}}\sqrt{\frac{L_R}{C_R}}. \quad (7)$$

The maximum power P_{MPP0} of the difference between P_{EMF}' and P_R' across a cycle therefore peaks when $v_{C(PK)}$ is v_{MPP0}:

$$P_{MPP0} \equiv P_{EMF}' - P_R'\big|_{v_{C(PK)}=v_{MPP0}} = \frac{v_{EMF(PK)}^2}{8R_{ESR}}. \quad (8)$$

For the conditions simulated in Fig. 4, $P_{EMF}' - P_R'$ in Fig. 6 maxes at P_{MPP0} or 521 µW when $v_{C(PK)}$ is v_{MPP0} or 2.8 V.

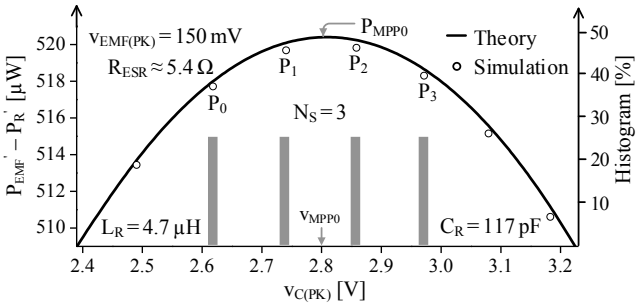

Fig. 6. Power profile in 1 cycle and histogram when skipping 3 half cycles.

When skipping N_S half cycles, $v_{C(PK)}$ climbs after every uncollected cycle. So $v_{C(PK)}$ cannot remain at the maximum power point v_{MPP0} across cycles. For example, when skipping 3 cycles like in Fig. 5 and centering v_C peaks about v_{MPP0}'s 2.8 V in Fig. 6, $v_{C(PK)}$ and $P_{EMF}' - P_R'$ between collection times are 2.6, 2.74, 2.86, and 2.97 V and 518, 520, 520, and 518 µW. So across $N_S + 1$ cycles, $P_{EMF} - P_R$ averages at 519 µW:

$$P_{EMF} - P_R = \left(\frac{1}{N_S+1}\right)\sum_{k=1}^{N_S+1}\left(P_{EMF(k)}' - P_{R(k)}'\right). \quad (9)$$

The sacrificial loss P_S that results is therefore

$$P_S = P_{MPP0} - \left(\frac{1}{N_S+1}\right)\sum_{k=1}^{N_S+1}\left(P_{EMF(k)}' - P_{R(k)}'\right) = f\left(v_{C(PK.k)}\right), \quad (10)$$

which varies with $v_{C(PK)}$ and half cycles skipped N_S.

The tank, in essence, collects across uncollected half cycles the output power P_O the battery would have otherwise received. The difference in $v_{C(PK)}$ between consecutive half cycles k – 1 and k therefore reflects the $0.5C_R v_{C(PK)}^2$ energy that the receiver supplied $P_{O(k)}$ across that half cycle k:

$$E_{O(k)} = 0.5T_O P_{O(k)} = 0.5C_R\left(v_{C(PK.k)}^2 - v_{C(PK.k-1)}^2\right). \quad (11)$$

So when $v_{EMF.R}$ peaks at 150 mV and oscillates at 6.78 MHz, $v_{C(PK)}$ grows from cycle to cycle like Fig. 7 shows.

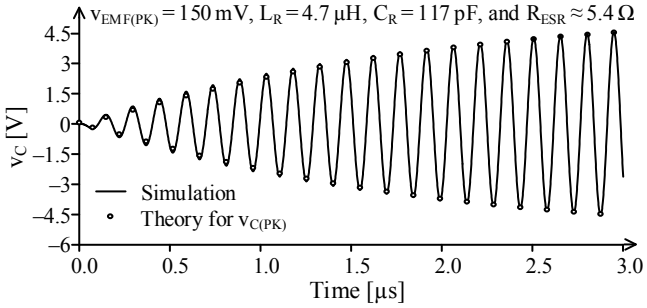

Fig. 7. Simulated capacitor voltage across uncollected half cycles.

As the number of half cycles skipped N_S rises, $v_{C(PK)}$'s spread widens. This means, more and more half cycles deviate further away from the maximum power point P_{MPP0}. In other words, the sacrificial loss P_S climbs with N_S. This is why $P_{EMF} - P_R$ in Fig. 8 is P_{MPP0} or 521 µW when the receiver collects every half cycle, because N_S is zero. And as N_S climbs, $P_{EMF} - P_R$ falls by P_S. So when N_S is 30, P_S is 62 µW.

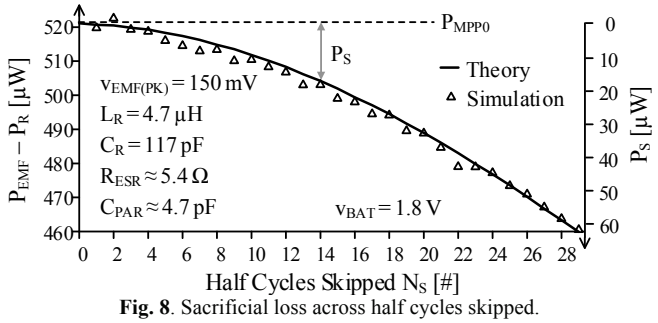

Fig. 8. Sacrificial loss across half cycles skipped.

Note that, unlike P_R and P_{SW}, P_S is not lost as heat. Since the receiver coil L_R is so small and distant, drawn P_{EMF} is much lower than the power the transmitter can actually supply. So P_{EMF} cannot over-damp the transmitter under these conditions. P_S is therefore power that the transmitter avails, but the receiver fails to collect.

IV. Maximum Output Power

Conduction, switching, sacrificial, and controller losses P_R, P_{SW}, P_S, and P_C ultimately limit how much of the drawn EMF power P_{EMF} the receiver outputs with P_O:

$$P_O = P_{EMF} - P_{LOSS} = P_{EMF} - P_R - P_{SW} - P_S - P_C \,. \quad (12)$$

When the receiver coil L_R is close to the transmitter, P_{EMF} can raise L_R's i_L to such a degree that P_R can overwhelm other losses to dominate P_{LOSS}. Under these conditions, the receiver should not sacrifice P_S for P_{SW}. Since $P_{EMF} - P_R$ across a half cycle peaks when $v_{C(PK)}$ is v_{MPP0}, the bridge should draw *every* half cycle just enough power P_O to keep $v_{C(PK)}$ at v_{MPP0}.

But when L_R is small and distant, as in embedded microsensors, P_{EMF} can be so low that P_{SW} and P_C can burn P_{EMF} entirely. Although skipping half cycles N_S reduces P_{SW} at the expense of P_S, reductions can outpace sacrifices up to an optimum number of skipped half cycles $N_{S(MPP)}$. So the bridge should draw every $N_{S(MPP)} + 1$ cycles just enough power to keep $v_{C(PK)}$ values centered about v_{MPP0}.

Under the same conditions simulated in Figs. 4–8, P_O in Fig. 9 maxes at $P_{O(MPP)}$ or 478 µW when N_S is $N_{S(MPP)}$ or 12. But since P_O varies little near $N_{S(MPP)}$, P_O is still 1% of $P_{O(MPP)}$ when N_S is 8–15. Without skipping, however, when N_S is 0 and all half cycle $v_{C(PK)}$'s are at v_{MPP0}, P_O is 2.7× lower.

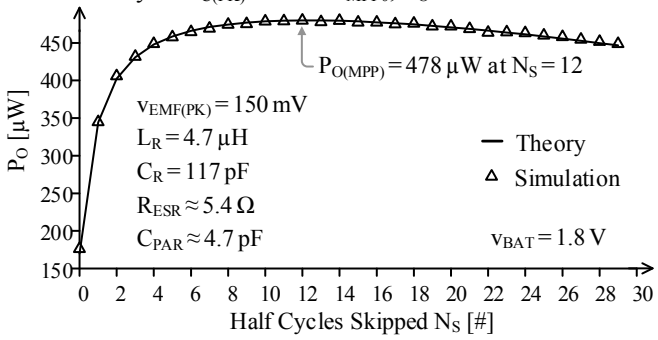

Fig. 9. Output power across half cycles skipped.

Other Implementations: Although [14]–[15] also skip half cycles, collections in [14]–[15] deplete the tank entirely. So after every collection, $v_{C(PK)}$ starts from nearly zero like Fig. 7 shows. For maximum output power, v_C should therefore rise high enough to keep $v_{C(PK)}$ values centered about v_{MPP0} in Fig. 6. For this, [15] would have to skip 38 half cycles to output no more than 378 µW. Collections in the scheme proposed here, however, only drain a fraction of the tank's energy. So $v_{C(PK)}$ values across skipped half cycles are closer to v_{MPP0}. This is why 378 µW is 26% lower than $P_{O(MPP)}$ in Fig. 9.

V. Conclusions

This paper proposes a power analysis and a skipping collection scheme for inductively coupled systems that outputs more power than previously reported strategies. Analysis and simulations show that skipping half cycles before partially draining the resonant tank in switched power receivers saves more power than it sacrifices when drawn EMF power P_{EMF} is low. This happens because, while conduction losses P_R scale down with P_{EMF}, switching losses P_{SW} do not. So with a lower collection frequency, P_{SW} savings outpace sacrificial losses. This is important when receiver coils are small and far from their transmitting counterparts, because they capture a small fraction of the magnetic flux generated. So skipping half cycles this way enables embedded microsensors in the body, equipment, and walls to collect more power from seldom-available transmitters that are not only near but also distant.

Acknowledgment

The authors thank Paul Emerson, Dr. Rajarshi Mukhopadhyay, Dr. Orlando Lazaro, and Texas Instruments for their support, feedback, and sponsorship.

References

[1] E.O. Torres, and G.A. Rincón-Mora, "Long-lasting, self-sustaining, and energy-harvesting system-in-package (SiP) wireless micro-sensor solution," *International Conference on Energy, Environment, and Disasters*, pp. 1–33, July 2005.

[2] J. Yoo, L. Yan, S. Lee, Y. Kim, and H.J. Yoo, "A 5.2 mw self-configured wearable body sensor network controller and a 12W wirelessly powered sensor for a continuous health monitoring system," *IEEE Journal of Solid-State Circuits,* vol. 45, no. 1, pp. 178–188, Jan 2010.

[3] S.H. Lee, M.Y. Su, M.C. Liang, Y.Y. Chen, C.H. Hsieh, C.M. Yang, H.Y. Lai, J.W. Lin, and Q. Fang, "A programmable implantable microstimulator SoC with wireless telemetry: Application in closed-loop endocardial stimulation for cardiac pacemaker," *IEEE Transactions on Biomedical Circuits and Systems,* vol. 5, no. 6, pp. 511–522, Dec. 2011.

[4] P.J. Chen, D.C. Rodger, S. Saati, M.S. Humayun, and Y.C. Tai, "Implantable parylene-based wireless intraocular pressure sensor," *IEEE International Conference on Micro Electro Mechanical Systems*, pp. 58–61, Jan. 2008.

[5] A.D. DeHennis and K.D. Wise, "A wireless microsystem for the remote sensing of pressure, temperature, and relative humidity," *Journal of Microelectromechanical Systems,* vol. 14, no. 1, pp. 12–22, Feb. 2005.

[6] M.A. Fonseca, J.M. English, M.V. Arx, and M.G. Allen, "Wireless micromachined ceramic pressure sensor for high-temperature applications," *IEEE Journal of Microelectromechanical Systems*, vol. 11, no. 4, pp. 337–343, Aug. 2002.

[7] O. Lazaro and G.A. Rincón-Mora, "180-nm CMOS wideband capacitor-free inductively coupled power receiver and charger," *IEEE Journal of Solid-State Circuits*, vol. 48, no. 11, pp. 2839–2849, Nov. 2013.

[8] N. Xing and G.A. Rincón-Mora, "Generating the highest power with a tiny and distant inductively coupled coil," *IEEE 25th International Symposium on Industrial Electronics (ISIE)*, pp. 447–480, Jun. 2016.

[9] M. Kiani, B. Lee, P. Yeon, and M. Ghovanloo, "A Q-Modulation Technique for Efficient Inductive Power Transmission", *IEEE Journal of Solid-States Circuits*, vol. 99, pp. 1–10, July 2015.

[10] A. Erdem, K. Colak, M. Bojarski, and D. Czarkowski, "A novel phase control of semi bridgeless active rectifier for wireless power transfer applications," *IEEE Applied Power Electronics Conference and Exposition*, pp. 3225–3231, Mar. 2015.

[11] B.X. Nguyen, D.M. Vilathgamuwa, G. Hock, B. Foo, P. Wang, A. Ong, U.K. Madawala, and T.D. Nguyen. "An efficiency optimization scheme for bidirectional inductive power transfer systems." *IEEE Transactions on Power Electronics*, vol. 30, no. 11, pp. 6310–6319, Nov. 2015.

[12] C.Y. Wu, X.H. Qian, M.S. Cheng, Y.A. Liang, and W.M. Chen, "A 13.56 MHz 40 mW CMOS high-efficiency inductive link power supply utilizing on-chip delay-compensated voltage doubler rectifier and multiple LDOs for implantable medical devices." *IEEE Journal of Solid-State Circuits*, vol. 49, no. 11, pp. 2397–2407, Nov. 2014.

[13] C.Y. Wu, X.H. Qian, M.S. Cheng, Y.A. Liang, and W.M. Chen, "A 13.56 MHz 40 mW CMOS high-efficiency inductive link power supply utilizing on-chip delay-compensated voltage doubler rectifier and multiple LDOs for implantable medical devices." *IEEE Journal of Solid-State Circuits*, vol. 49, no. 11, pp. 2397–2407, Nov. 2014.

[14] B. Lee, P. Yeon, and M. Ghovanloo, "A multi-cycle Q-modulation technique for wirelessly-powered biomedical implants." *IEEE Biomedical Circuits and Systems Conference,* pp. 1–4, Oct. 2015.

[15] H.S. Gougheri and M. Kiani, "Current-based resonant power delivery with multi-cycle switching for extended-range inductive power transmission," *IEEE Transactions on Circuits and Systems I*, vol. 63 no. 9, pp. 1543–1552, Sep, 2016.